Enhanced response of global wetland methane emissions to the 2015-2016 El Niño-Southern Oscillation event

Zhen Zhang[1,2], Niklaus E. Zimmermann[2,3], Leonardo Calle[4], George Hurtt[1], Abhishek Chatterjee [5,6], Benjamin Poulter[5]

[1]Department of Geographical Sciences, University of Maryland, College Park, MD 20740, USA

[2]Dynamic Macroecology, Swiss Federal Research Institute WSL, Zürcherstrasse 111, Birmensdorf 8903, Switzerland

[3]Department of Environmental System Science, Swiss Federal Institute of Technology ETH, Zürich 8092, Switzerland

[4]Department of Ecology, Montana State University, Bozeman, MT 59717, USA

[5]Biospheric Sciences Laboratory, NASA Goddard Space Flight Center, Greenbelt, MD 20771, USA

[6]Universities Space Research Association, Columbia, MD 21046, USA

Abstract: Wetlands are thought to be the major contributor to interannual variability in the growth rate of atmospheric methane (CH_4) with anomalies driven by the influence of the El Niño-Southern Oscillation (ENSO). Yet it remains unclear whether (i) the increase in total global CH_4 emissions during El Niño versus La Niña events is from wetlands and (ii) how large the contribution of wetland CH_4 emissions is to the interannual variability of atmospheric CH_4. We used a terrestrial ecosystem model that includes permafrost and wetland dynamics to estimate CH_4 emissions, forced by three separate meteorological reanalyses and one gridded observational climate dataset, to simulate the spatio-temporal dynamics of wetland CH_4 emissions from 1980-2016. The simulations show that while wetland CH_4 responds with negative annual anomalies during the El Niño events, the instantaneous growth rate of wetland CH_4 emissions exhibits complex phase dynamics. We find that wetland CH_4 instantaneous growth rates were declined at the onset of the 2015-2016 El Niño event but then increased to a record-high at later stages of the El Niño event (January through May 2016). We also find evidence for a step increase of CH_4 emissions by 7.8±1.6 Tg CH_4 yr^{-1} during 2007-2014 compared to the average of 2000-2006 from simulations using meteorological reanalyses, which is equivalent to a ~3.5 ppb yr^{-1} rise in CH_4 concentrations. The step increase is mainly caused by the expansion of wetland area in the tropics (30°S-30°N) due to an enhancement of tropical precipitation as indicated by the suite of the meteorological reanalyses. Our study highlights the role of wetlands, and the complex temporal phasing with ENSO, in driving the variability and trends of atmospheric CH_4 concentrations. In addition, the need to account for uncertainty in meteorological forcings is highlighted in addressing the interannual variability and decadal-scale trends of wetland CH_4 fluxes.

Introduction

Methane (CH_4) is a potent greenhouse gas and has contributed to ~20% of observed warming since pre-industrial times (IPCC, 2013). Atmospheric CH_4 concentrations have risen from preindustrial levels of 715 parts per billion (ppb) since the 1800s (Etheridge *et al.*, 1998; MacFarling Meure *et al.*, 2006) to current global concentration of ~1847 ppb, a 2.5-fold increase, primarily driven by anthropogenic activities (Kirschke *et al.*, 2013), e.g. fossil fuel activities, agriculture, and also by the biogeochemical feedbacks of natural processes to climate change (Arneth *et al.*, 2010; Tian *et al.*, 2016; Saunois *et al.*, 2016). However, the variability in the annual growth rate of atmospheric CH_4 is strongly related to the climatic sensitivity of biogenic CH_4 sources, of which global wetland CH_4 comprises 60-80% of natural emissions (Quiquet *et al.*, 2015; Hopcroft *et al.*, 2017) and this large role is likely to persist into the future (Zhang *et al.*, 2017b). Thus, interannual variability in the growth rate of atmospheric CH_4 is largely affected by the response of global wetland CH_4 emissions to the year-to-year mode of global climate variability such as the El Niño-Southern Oscillation (ENSO). ENSO is one of the largest climate phenomena that drives carbon dynamics and their anomalies across large portions of the globe (Chatterjee *et al.*, 2017).

El Niño, the positive phase of ENSO, influences water- and carbon- fluxes of tropical terrestrial ecosystems through a change in patterns of atmospheric pressure and sea surface temperature (Philander 1990). These changes induce strong warming and reduced precipitation patterns by shifting the Intertropical Convergence Zone southward, causing amplified wildfires (Worden *et al.*, 2013) and reduced wetland areal extent and CH_4 emissions (Hodson *et al.*, 2011). Tropical wetlands, which comprise 50-70% of global wetland CH_4 emissions (Bousquet *et al.*, 2006), are similarly influenced by the periodic variations of air temperature and precipitation related to ENSO phases (Pison *et al.*, 2013). Atmospheric measurements of CH_4 provide evidence that the growth rate of global CH_4 concentrations can rise during strong El Niño years (Nisbet *et al.*, 2016; Bousquet *et al.,* 2006), but terrestrial biogeochemical models suggest that tropical and global wetland CH_4 emissions are usually found to decrease during El Niño (Hodson *et al.*, 2011; Zhu *et al.*, 2017; Ringeval *et al.*, 2014).

At decadal time scales, the relationship between the annual CH_4 growth rate and variability in global wetland CH_4 emissions is not fully agreed upon, and the observed pause in the growth rate during 2000-2006 and subsequent return of the growth rate since 2007 (Nisbet *et al.*, 2014) is not fully understood. A recent study suggests that global wetlands have played a limited role during the renewed rise of the growth rate through 2012 (Poulter *et al.*, 2017). However, isotopic measurements indicate that the resumed increase in the growth rate could originate either from biogenic sources (Schwietzke *et al.,* 2016) like tropical wetlands (Nisbet *et al.*, 2016), from agricultural sources (Schaefer *et al.*, 2016), or from the combined effect of decreased biomass burning (Worden *et al.,* 2017) and increased fossil-fuel emissions (Helmig *et al., 2016*). In addition, simple-box models and more complex atmospheric inversion models can attribute the recent CH_4 change to varying hydroxyl radical (OH) concentration, the major CH_4 sink in the atmosphere (Turner *et al.*, 2017; Rigby *et al.*, 2017). Our poor understanding of wetland CH_4 responses at annual to decadal time scales calls for revisiting the role of relationships between climate forcings and wetland CH_4 fluxes to help reconcile top-down and bottom-up methodologies.

Previous El Niño anomalies, in years 1982-1983, 1997-1998, and 2015-2016, had significant impacts on terrestrial ecosystems and these events were considered key drivers of the atmospheric CO_2 growth rate variability (Liu *et al.*, 2017). The most recent El Niño event (2015-2016) caused unprecedented warming and extreme drought over most of the Amazonia regions (Jiménez-Muñoz *et al.*, 2016; L'Heureux *et al.*, 2016; Lim *et al.*, 2017; Chatterjee *et al.*, 2017). The occurrence of this extreme El Niño event disrupted regional ecosystems, causing sharp increases in atmospheric CO_2 concentrations (Betts *et al.*, 2016) and a doubling of fire-induced emissions in Southeast Asia (Whitburn *et al.*, 2016). The more recent El Niño event may have also contributed to record warming during 2015 and the first third of 2016, with global air temperature at 0.94°C above the 20th century mean annual average (http://www.ncdc.noaa.gov/sotc/global/201613, last access in August 2017). Exactly how much the 2015-2016 ENSO phenomenon has impacted global wetland CH_4 emissions and to what extent it has affected the annual growth rate of atmospheric CH_4 concentration remains unknown due to challenges in monitoring and modeling.

Here, we analyze the relationship between ENSO phase and wetland CH_4 emissions by addressing two main questions: First, how does ENSO, with particular attention to the ENSO event in 2015-2016, affect the interannual variability of CH_4 emissions from global wetlands? Second, what are the major mechanisms that link wetland CH_4 emissions to the atmospheric increases observed since 2007?

Methods

We use a process-based ecosystem model LPJ-wsl (Lund-Potsdam-Jena model, *WSL* version) forced with four different meteorological forcings to simulate wetland CH_4 emissions from 1980 to 2016. These drivers include one station-based monthly geo-interpolation dataset (CRU) and three meteorological reanalyses products (Table 1). We use multiple climate datasets to investigate uncertainty from meteorological forcing driving simulated atmospheric CH_4 concentrations, and hence, to better characterize CH_4 variation in response to climate variations.

LPJ-wsl (Poulter *et al.*, 2011) is a process-based dynamic global vegetation model (DGVM) developed for studying terrestrial ecosystems, based on an earlier LPJ core model (Sitch *et al.*, 2003). The version of the model applied in this study includes a new hydrology model, TOPMODEL, to determine wetland area and its inter- and intra-annual dynamics (Zhang et al., 2016), a permafrost and dynamic snow model (Wania et al., 2009), and a prognostic wetland CH_4 emission model (Hodson et al., 2011), each of which is incorporated into the LPJ-wsl framework with explicit representation of the effects of snow and freeze/thaw cycles on soil temperature and moisture and thus CH_4 emissions (Zhang *et al.*, 2016). We apply an empirical model to estimate CH_4 emissions in the model which is based on soil respiration, inundated area, and a temperature-based ecosystem emission efficiency (Christensen *et al.*, 1996). Soil respiration is modelled empirically in response to temperature and soil moisture based on an Arrhenius type equation where varying effective activation energies for respiration and a dampening of the temperature sensitivity (Q_{10}) due to acclimation were considered (Sitch *et al.,* 2003). The simulated dynamics of wetland area and CH_4 emissions have been evaluated against large-scale observations in previous studies (Hodson *et al.*, 2011; Zhang *et al.*, 2016; Zhang *et al.*, 2017b). Here, we calibrated temperature-modified CH_4 emitting factors by scaling simulated global estimates to match 172 Tg CH_4 yr^{-1} in 2004, which was estimated from an independent atmospheric inversion study (Spahni et al., 2011), and is in agreement with independent satellite-based methods from Bloom *et al.* (2010). We improved inundation estimates by calibrating the TOPMODEL parameter 'maximum inundation potential' (F_{max}) (Zhang et al., 2016) using an independent inundation dataset (Poulter *et al.*, 2017) that was derived from a satellite-based Surface Water Microwave Product Series (SWAMPS) (Schroeder *et al.*, 2015), an inventory-based dataset Global Lakes and Wetlands Database (GLWD) (Lehner and Döll, 2004), and a regional wetland map derived from satellite retrievals for Amazonia (Hess et al., 2015). To avoid confusion regarding double counting (Thornton *et al.*, 2016), we clarify that our simulated wetland area includes seasonally inundated wetlands, e.g. floodplains, and permanently inundated vegetated wetlands, but excludes rice agriculture, non-vegetated reservoirs, medium to large sized lakes, rivers, and coastal wetlands that are not accounted for by the GLWD.

The climate datasets included the monthly meteorology from the Climate Research Unit (CRU) TS 3.25 (Harris *et al.*, 2014) and three state-of-the-art metrological reanalysis products. The reanalysis products were comprised of 1-hourly reanalysis Modern-Era Retrospective analysis for Research and Applications Version 2 (MERRA2) (Gelaro *et al.*, 2017) from the NASA Global Modeling and Assimilation Office (GMAO), 6-hourly ERA-Interim (ERA-I) (Dee *et al.*, 2011) from the European Centre for Medium-Range Weather Forecasts (ECMWF) data assimilation system and, and lastly, a 6-hourly Japanese 55-year Reanalysis (JRA-55) (Kobayashi *et al.*, 2015) from the Japan Meteorological Agency (JMA). The reanalysis data (total precipitation, 2m air temperature, downward shortwave radiation, and downward longwave radiation) were aggregated to a common daily time-step and downscaled to 0.5° spatial resolution grid using first order conservative interpolation. The soils dataset we used was the Harmonized World Soil Database v1.2 (Nachtergaele *et al.,* 2008) and using pedotransfer functions of the surface soil texture (Cosby *et al.,* 1984) to estimate volumetric water holding capacity. For the monthly CRU data, LPJ-wsl was set up to use a wet-day frequency dataset, a weather generator (Geng *et* *al.*, 1986) to generate daily precipitations, and a set of simplified equations with monthly cloud cover as input to calculate daily photosynthetically active radiation flux and potential evapotranspiration (Prentice *et al.*, 1993). Additional details of the climate datasets and model experiments are in the Supplementary Material (Table S1). The LPJ-wsl state variables (i.e., carbon in vegetation, litter, and soils) were simulated to reach equilibrium by using a 1000-year spinup, with fire dynamics, and a 398-year spinup for land use change using Land-Use Harmonization dataset (LUHv2) (Hurtt *et al. 2011*). Spin-up was done using randomly selected climate inputs from 1901-1930 for CRU and 1980-2000 for reanalysis with fixed atmospheric CO_2 to the 1860 value. After equilibrium, a transient simulation with fire effects and varying land cover was performed for the years 1901-2016 (for CRU) and 1980-2016 (for reanalysis), forced with changing climate conditions and varying atmospheric CO_2 concentration (https://www.esrl.noaa.gov/ccgg/trends, last access at August 2017). The simulations consider gross land-use transitions (with no wood harvest) with primary and secondary lands treated separately (for details, see Arneth *et al.,* 2017), where the soil moisture and soil respiration were calculated by fraction-weighting individual land stands within a grid cell.

We used the Multivariate ENSO index (MEI) for representing the ENSO strength (Wolter and Timlin, 1998). The MEI index represents the first unrotated principal component of the combined, normalized fields of the primary climate variables observed over the tropical Pacific, reflecting a global signal of climate-land-atmosphere interaction for both El Niño and La Niña events. Given that previous studies (Fang *et al.*, 2017; Liu *et al.*, 2017) have shown a hysteresis in the Earth systems response to changes in temperature and precipitation patterns, we carried out a cross-correlation analysis to examine possible time-lag effects of wetland CH_4 response to El Niño events.

To test whether annual wetland CH_4 anomalies contributed to the growth rate of atmospheric CH_4, we compared our results against the annual mean global CH_4 growth rate and monthly CH_4 trend derived from NOAA/ESRL (https://www.esrl.noaa.gov/gmd/ccgg/flask.php, last access at August 2017). We then used the first derivative of spline-smoothed monthly wetland CH_4 anomalies to calculate the wetland CH_4 instantaneous growth rate. The time series of CH_4 concentration measurements, derived from NOAA cooperative air sampling network, were processed with a curve fitting method (Thoning *et al.*, 1989) that decomposes the full signal into a long-term growth rate fit by a polynomial function, seasonal oscillations by a harmonic function, and a low pass digital filter to retain interannual and short-term variations. From the decomposed signal, we derived component signals such as trend, growth rate, and annual amplitude. The CH_4 amplitude of the seasonal cycle from Mauna Loa surface site (MLO: 19.53°N, 155.58°W) in NOAA/ESRL was applied to the analysis as an indicator of the strength of CH_4 seasonality in the Northern Tropics, where CH_4 amplitude is mainly controlled by OH and fluxes from the land biosphere. Given that wetlands contribute the largest fraction of natural CH_4 sources and that the interannual variability of OH is relatively small (Montzka *et al.*, 2011), the changing trends in the CH_4 amplitude consequently imply that the variation in the trend is largely affected by changing CH_4 dynamics in wetland ecosystems. To test whether the shifting spatio-temporal patterns of simulated wetland CH_4 dynamics are consistent with observations, we compared the observed MLO CH_4 amplitude with simulated wetland CH_4 amplitude, which was calculated as the difference between annual maxima and minima in spline-smoothed monthly wetland CH_4 anomalies.

For evaluation of wetland areal changes we used terrestrial water storage (TWS) anomalies, observed by the Gravity Recovery and Climate Experiment (GRACE) satellite measurement, as a proxy for groundwater storage and surface inundation (Bloom *et al.*, 2012; Boening *et al.*, 2012). We used the Level-3 monthly 'solutions', version RL05, from Geo Forschung Zentrum (GFZ), the University of Texas Center for Space Research (CSR), and the Jet Propulsion Laboratory (JPL) from April 2002 to December 2016 to analyze the temporal variations of water mass in the tropics. The monthly TWS was multiplied by a spatial grid of scaling coefficients derived from post-processing of GRACE observations (Landerer and Swenson, 2012) to restore the signals attenuated in the processing at small spatial scales. We used the ensemble mean of monthly TWS from three different products in the analysis because the ensemble mean was the most effective in reducing the noise in gravity fields solutions from GRACE data (Sakumura *et al.*, 2014).

Results and Discussion

Long-term response of wetland CH_4 to ENSO

The ensemble climate simulations indicate a strong link between ENSO and wetland CH_4 emissions, with higher emissions during La Niña and lower emissions during El Niño (Figure 1a). We find significant negative correlations (r_{MERRA2}=-0.51, r_{ERA-I}=-0.36, r_{CRU}=-0.45, r_{JRA-55}=-0.35, d.f.=443, $p < 0.01$) between the ENSO MEI index and monthly wetland CH_4 anomalies, regardless of the climate data used in the simulations. This is consistent with findings from bottom-up modeling estimates (Hodson *et al.*, 2011; McNorton *et al.*, 2016; Zhu *et al.*, 2017), atmospheric modeling (Pison *et al.*, 2013; Chen and Prinn, 2006) and satellite observations. For instance, the atmospheric CH_4 variations of the mid-troposphere measured by the Infrared Atmospheric Sounding Interferometer (IASI) aboard METOP satellite, and by the Atmospheric Infrared Sounder (AIRS) aboard NASA's Aqua satellite, also show higher increases in 2007-2008 and 2010-2011 when strong La Niña events occurred (Xiong *et al.*, 2016). Airborne-based estimates of the interannual variability of CH_4 fluxes for eastern Amazon Basin also provide ancillary evidence that the CH_4 emissions are greatest in 2008, a year of La Niña phase (Basso *et al.*, 2016). Recent satellite observations from the Greenhouse gases Observing SATellite (GOSAT) also suggest large-scale fluctuations in atmospheric CH_4 during ENSO events, indicating that wetland CH_4 emissions are ~5% higher during La Niña events (Pandey *et al.*, 2017). The increase in CH_4 emissions from wetlands during La Niña can be attributed to a large increase in flood extent, primarily over tropical areas (including SE Australia, northern South America, and Southeast Asia) (Boening *et al.*, 2012), whereas the decreases during El Niño are possibly due to drought-induced decreases in flooded area. All of the evidence above suggests a robust negative relationship between annual anomalies of wetland CH_4 emissions and ENSO events, i.e., positive anomalies during La Niña and vice versa.

However, negative anomalies of annual wetland CH_4 emissions do not necessarily lead to a decrease in the instantaneous growth rate of wetland CH_4 emissions during El Niño. We find that the growth rate of wetland CH_4 emissions is initially decreased but then is in a rising phase during the later stages of strong El Niño events. Although, the amplitude of the rising varied depending on which meteorological forcing was used in the simulations (Figure 1b). This is mainly because strong El Niño events drive negative wetland CH_4 growth rates at the beginning of the ENSO anomaly, but then the growth rate rapidly recovers to positive values. Despite positive atmospheric methane growth rate correlations with El Niño events, the general decline in wetland area causes declines in wetland CH_4 emissions at the beginning of strong El Niño phases. The high temperatures over the tropics strongly increase the CH_4 growth rate due to higher soil decomposition rates during the later stages of the 2015-2016 El Niño event. Cross-correlation analyses between the monthly growth rate of wetland CH_4 emissions and the MEI index suggest that the peak correlation occurs at a 3-month lag (when ENSO leads $\Delta CH_4/\Delta t$) for the globe. As expected, the timing of wetland response to ENSO varies regionally, where Tropical Asia and Tropical South America exhibit a ~4 month lag and no lag, respectively (Figure S1). The Interannual Variability (IAV) of wetland CH_4 emissions is dominated by the Tropics (30°S-30°N) with relatively small contributions from the Northern Hemisphere (Figures 1c, 1d). MERRA2 showed the highest IAV among all four simulations, whereas the CRU-based simulation had the lowest IAV. The rise of wetland CH_4 emission growth rate is consistent with the observed spikes of atmospheric CH_4 growth rates during strong El Niño events (Nisbet *et al.,* 2016).

Impact of 2015-2016 El Niño on wetland CH_4

The amplitude of instantaneous growth in wetland CH_4 emissions during the 2015-2016 El Niño was higher than that in the previous periods 1982-1983 and 1997-1998, suggesting an increased sensitivity of wetland CH_4 in response to the recent El Niño (Figure 1b). Our results captured the magnitude of this large increase in wetland CH_4 emissions with an instantaneous growth rate of ~7.6±1.6 Tg CH_4 yr^{-1} during 2015-2016 El Niño. The meteorological datasets drove instantaneous growth rates that ranged between 9.2 Tg CH_4 $month^{-1}$, 8.6 Tg CH_4 yr^{-1}, 7.2 Tg CH_4 yr^{-1}, and 5.5 Tg CH_4 yr^{-1} using MERRA2, JRA-55, CRU, and ERA-I, respectively. Although the 2015-2016 El Niño was not as strong as the 1997-1998 El Niño according to the MEI index (~3 in 1997-1998 and ~2.5 in 2015-2016), the combined effect of rising CO_2 concentrations and high temperatures most likely amplified the impact, causing 1.8 times the maximum growth rate of CH_4 of the 1997-1998 El Niño event (mean growth rate of ~4.2±1.4 Tg CH_4 yr^{-1} for the respective time period).

The spatial distribution of wetland CH_4 anomalies demonstrated that the large increases in soil respiration drove the strong growth rate and occurred during the March-April-May (MAM) season in 2016 as a consequence of warming and droughts in the wet seasons (October 2015 - May 2016) (Figure 2). There was a widespread increase in CH_4 emissions over western Amazonia, mainly attributed to increased soil respiration. Despite a large decline in wetland extent due to severe drought, significant positive anomalies in CH_4 emission peaked across the western Amazonian basin, likely due to high temperatures. Temperature is the primary climatic variable driving the increasing long-term trend in CH_4 emissions (Zhang *et al.*, 2017b). However, precipitation is the dominant climatic variable regulating interannual variability in CH_4 emissions by altering the inundation extent and creating anaerobic conditions suitable for methanogenesis in the tropics (Zhang *et al.*, 2017b).

Wetland CH_4 trends between 2000-2006 and post-2007

Using the meteorological reanalysis data, we find evidence for a step increase in global annual wetland emissions between the periods of 2007-2014 relative to that of 2000-2006 (Figure 3a). These simulations suggest that the average annual CH_4 emissions from 2007-2014 increased by ~7.8±1.6 Tg CH_4 yr^{-1} compared to the average of 2000-2006, which is equivalent to an increase in the growth rate of up to ~ 3.5 ppb CH_4 yr^{-1} for the post-2007 period, or about half of the observed increase in concentrations. The CRU-based simulation in this study did not show a strong step-increase between these two periods, suggesting only a marginal contribution from wetlands with a 1.5 Tg CH_4 yr^{-1} increase in the post-2007 growth rate. This is consistent with findings from an ensemble modeling experiment using CRU as a forcing dataset, which found no significant increase of global wetland CH_4 emissions during the period of renewed atmospheric CH_4 growth (Poulter *et al.*, 2017). Another recent atmospheric modeling study, also using CRU as forcing for their prior inputs, likewise suggested that wetlands made only a small contribution to the post-2007 growth at ~1 ppb/yr (McNorton *et al.*, 2016). In contrast to the CRU simulations just listed, all our simulations using meteorological reanalysis data suggest that more than 90% of the increase in the growth rate of wetland CH_4 is from the Tropics (Table 2), and mainly due to increases in precipitation across South America, Tropical Africa, and Southeast Asia since 2007. MERRA2-based simulations suggest that the post-2007 rise in global CH_4 concentrations primarily comes from South America and Tropical Africa, whereas ERA-I and JRA-55 identify South America as the largest contributor to the CH_4 growth rate (Figure S2).

The different IAV patterns of CH_4 emissions among these simulations suggest considerable uncertainties in CH_4 emissions due to climate drivers (Figure 3a). The model experiments demonstrated that the discrepancy originates mainly from different model behavior when using products like CRU and meteorological reanalyses like MERRA2, ERA-I, and JRA-55, regardless of the temporal resolution of climate inputs used (Figure S3). We found only minor differences using a daily or monthly temporal resolution, which likely reduced uncertainties from applying the simulated weather generator and thus show that the weather generator covered the internal climatic variability at monthly scale. The importance of considering uncertainty of climate forcing was also reflected in the representation of the seasonal cycle of CH_4 emissions. The comparison of simulated CH_4 emissions with independent estimates using an atmospheric model STILT based on CARVE airborne experiments (Zona *et al.*, 2016) suggested a dominant role of climate forcings in capturing CH_4 seasonality in arctic regions (Figure 3b). MERRA2, ERA-I, and JRA-55 underestimated the peak CH_4 emission in growing season but were able to capture the general seasonal cycle in CH_4 emissions for the North Slope of Alaska, while CRU-based estimates failed to reproduce a similar pattern. The seasonal cycle of CH_4 emissions was also generally underestimated by most bottom-up models that used CRU climate data in a synthesis modeling experiment (Melton *et al.*, 2013), highlighting the need to better constrain the CH_4 emissions by taking into account several datasets that represent climate forcing uncertainty.

Sensitivity of wetland CH_4 emissions to ENSO

To further investigate whether the influence of ENSO on global wetland CH_4 fluctuation was strengthening, we evaluated the average sensitivity of simulated wetland CH_4 emissions and wetland areas in the tropics to ENSO events. To this means we calculated the ratio of the annual anomaly of CH_4 emission/wetland area to the annual MEI index for three different time periods, 1980-1999, 2000-2006, and 2007-2016 (Figure 4). We observed a minor change in the sensitivity of CH_4 emissions and wetland areas between 1980-1999 and 2000-2006, which suggests a subtle change in the response of global wetland CH_4 emissions to increasing global temperatures. However, the sensitivity of the modeled results strongly increased for the period of 2007-2016 relative to the two previous time periods. The sensitivity in CH_4 emissions increased by ~200% in MERRA2, ERA-I, and JRA-55, whereas the CRU run resulted in a lower percent increase (42%) compared to the other model experiments. The concurrent increase in the sensitivity of CH_4 emissions and wetland areas indicates that the increase of CH_4 emissions since 2007 can mainly be attributed to an increased sensitivity of wetland areas, which was driven by the changing precipitation patterns found in meteorological reanalysis products. The GRACE measurement for relative equivalent water storage confirms the large increase for the period of 2007-2014 compared to earlier periods (Figure 5), suggesting that our simulated increases in tropical wetland areas are robust. All of the modeled wetland areas have significant correlations (r_{MERRA2}=0.59, $r_{ERA\text{-}I}$=0.59, r_{CRU}=0.56, $r_{JRA\text{-}55}$=0.5, d.f.=176, p <0.01) with GRACE TWS, and suggest a ~150 10^3 km^2 increase in inundation over time period of 2007-2014. This also implies that, despite an observed decline in open waters in the tropics (due to the anthropogenic effect from denser populations and impacts from human activities for the period of 1990s and early 2000s (Prigent *et al.*, 2012)), the enhanced precipitation since 2007 (Sun *et al.,* 2017; Rodell *et al.,* 2018) was primarily related to the ENSO phase over Tropical land, which has affected wetland patterns and CH_4 emissions globally.

Relationship between wetland CH_4 and atmospheric growth rate

There was a statistically significant ($p < 0.10$) positive trend in the simulated annual amplitude of wetland CH_4 emissions, suggesting an increasingly enhanced sensitivity of wetland CH_4 emissions to climate change in recent decades (Figure 6). All model simulations indicated positive trends of the annual amplitude of wetland CH_4 emissions with small differences depending on climate forcings. These simulated positive trends are consistent with observed trends in CH_4 amplitude at the MLO site, for which MERRA2, ERA-I, and JRA-55 runs were correlated with MLO observations (r_{MERRA2}=0.36, r_{ERA-I}=0.42, r_{CRU}=0.29, r_{JRA-55}=0.37, d.f. = 30, $p < 0.05$) and only CRU-based simulations showed a weak correlation between wetland CH_4 emissions and enhanced global CH_4 seasonality. These significant correlations suggest relationships between atmospheric CH_4 seasonality and natural wetland emissions, despite the major role of OH in determining CH_4 seasonality. The increasing trends in CH_4 amplitude also imply a high likelihood that there is an underlying shift of CH_4 seasonality in wetland ecosystems and this shift in seasonality is likely greatest in tropical regions.

We found a small, but significant, positive correlation between annual wetland CH_4 emissions and the annual atmospheric CH_4 growth rate in simulations forced by the daily meteorological datasets MERRA2 (r= 0.31, d.f.= 33, $p < 0.1$), ERA-I (r= 0.36, d.f.=33, $p < 0.1$), and JRA-55 (r=0.38, d.f.=33, $p < 0.05$) for the period of 2000-2015, whereas no significant correlation was found in CRU-based runs (r=0.07, d.f.= 33, $p>0.75$). For the period of 1980-1999, none of the simulations showed a significant correlation with the annual atmospheric CH_4 growth rate. The atmospheric CH_4 growth rate is not exclusively a result of changes in wetland emissions, but rather due to a combined influence of anthropogenic and natural sources, and also due to a hydroxyl radical sink (Turner *et al.*, 2017; Rigby *et al.*, 2017). Recent studies have reported an increase in annual CH_4 emissions from global livestock (Wolf *et al.*, 2017) and an expansion of agricultural areas for rice paddies in Southern Asia (Zhang *et al.*, 2017a), a region where precipitation has largely increased since 2007. Thus, we hypothesize that a combination of tropical wetlands and agricultural sources are likely responsible for the resumed growth rate of atmospheric CH_4 concentrations, which is consistent with the depletion in the global isotopic signature in $^{13}CH_4$ (Schaefer *et al.*, 2016) and with regional measurements of $^{13}CH_4$ in the Tropics (Nisbet *et al.,* 2016).

Conclusions

We demonstrate that global wetland CH_4 emission anomalies are strongly related to ENSO variability using an extended, multi-meteorological ensemble. At sub-annual time-scales, we also found that the instantaneous growth rate of wetland CH_4 anomalies was positively correlated with ENSO strengths, which provides an explanation for the observed rise of atmospheric CH_4 growth rate during strong El Niño events. The ongoing warming trend, as well as the shifting patterns of global precipitation, has likely had a significant impact on increasing global CH_4 interannual variability. The strong El Niño event in 2015-2016, associated with extreme heat and drought over the Amazonian regions, caused record-high growth rates of wetland CH_4 emissions compared to the previous three decades. We also found an increasing sensitivity of wetland CH_4 emissions to ENSO oscillation since 2007, which we attribute to increases in the areal extent of tropical wetlands from increased precipitation. Our study also highlights the need to account for uncertainty in the climate forcing for estimating wetland CH_4 emissions.

Acknowledgements

This study is funded in part by the Gordon and Betty Moore Foundation through Grant GBMF5439 "Quantifying Sources and Sinks in the Global Methane Cycle" to Zhen Zhang, George Hurtt, and Benjamin Poulter. We thank the Competence Center Environment and Sustainability (CCES) project Modeling and Experiments on Land-Surface Interactions with Atmospheric Chemistry and Climate Phase 2 (MAIOLICA2) #42-01, and the National Natural Science Foundation of China (T411391009) for additional funding. We further thank NASA for preparing the MERRA2 dataset, the European Centre for Medium-Range Weather Forecasts for preparing the ERA-Interim dataset, the Japan Meteorological Agency for preparing the Japanese 55-year Reanalysis (JRA-55) dataset, and the Climate Research Unit at the University of East Anglia for providing the CRU dataset. We finally thank the NOAA ESRL Global Monitoring Division for providing CH_4 measurements. We thank Sara H. Knox and Katelyn Dolan for constructive comments on the manuscript.

Data availability

The data that support the findings of this study are available upon request, for access please contact Z. Zhang (yuisheng@gmail.com). Atmospheric CH_4 concentration datasets were obtained from the NOAA ESRL GMD Carbon Cycle Cooperative Global Air Sampling Network (https://www.esrl.noaa.gov/gmd/ccgg/flask.php, last access at August 2017). The annual mean global CH_4 growth rate and monthly trend were derived from NOAA/ESRL ((www.esrl.noaa.gov/gmd/ccgg/trends_ch4/). Terrestrial Water Storage products were derived from the GRACE website (https://grace.jpl.nasa.gov/data/get-data/, last accessed on October 2017). We used the multivariate ENSO index (MEI) (https://www.esrl.noaa.gov/psd/enso/mei/, last access at October 2017) as indices for representing ENSO strength.

References:

Arneth A, Harrison S P, Zaehle S, Tsigaridis K, Menon S, Bartlein P J, Feichter J, Korhola A, Kulmala M, O'Donnell D, Schurgers G, Sorvari S and Vesala T 2010 Terrestrial biogeochemical feedbacks in the climate system *Nature Geosci* **3** 525-32

Basso L S, Gatti L V, Gloor M, Miller J B, Domingues L G, Correia C S C and Borges V F 2016 Seasonality and interannual variability of CH_4 fluxes from the eastern Amazon Basin inferred from atmospheric mole fraction profiles *Journal of Geophysical Research. Atmospheres* **121** 168-84

Betts R A, Jones C D, Knight J R, Keeling R F and Kennedy J J 2016 El Nino and a record CO_2 rise *Nature Clim. Change* **6** 806-10

Bloom A A, Palmer P I, Fraser A and Reay D S 2012 Seasonal variability of tropical wetland CH_4 emissions: the role of the methanogen-available carbon pool *Biogeosciences* **9** 2821-30

Bloom A A, Palmer P I, Fraser A, Reay D S and Frankenberg C 2010 Large-Scale Controls of Methanogenesis Inferred from Methane and Gravity Spaceborne Data *Science* **327** 322-5

Boening C, Willis J K, Landerer F W, Nerem R S and Fasullo J 2012 The 2011 La Niña: So strong, the oceans fell *Geophysical Research Letters* **39** L19602

Bousquet P, Ciais P, Miller J B, Dlugokencky E J, Hauglustaine D A, Prigent C, Van der Werf G R, Peylin P, Brunke E G, Carouge C, Langenfelds R L, Lathiere J, Papa F, Ramonet M, Schmidt M, Steele L P, Tyler S C and White J 2006 Contribution of anthropogenic and natural sources to atmospheric methane variability *Nature* **443** 439-43

Chatterjee A, Gierach M M, Sutton A J, Feely R A, Crisp D, Eldering A, Gunson M R, O'Dell C W, Stephens B B and Schimel D S 2017 Influence of El Niño on atmospheric CO_2 over the tropical Pacific Ocean: Findings from NASA's OCO-2 mission *Science* **358**

Chen Y-H and Prinn R G 2006 Estimation of atmospheric methane emissions between 1996 and 2001 using a three-dimensional global chemical transport model *Journal of Geophysical Research: Atmospheres* **111** 2156-202

Christensen T R, Prentice I C, Kaplan J, Haxeltine A and Sitch S 1996 Methane flux from northern wetlands and tundra *Tellus B* **48** 652-61

Cosby, B J, Hornberger, G M, Clapp, R B, and Ginn, T R 1984 A Statistical Exploration of the Relationships of Soil MoistureCharacteristics to the Physical Properties of Soils, Water Resour. Res., 20, 682–690.

Dee D P, Uppala S M, Simmons A J, Berrisford P, Poli P, Kobayashi S, Andrae U, Balmaseda M A, Balsamo G, Bauer P, Bechtold P, Beljaars A C M, van de Berg L, Bidlot J, Bormann N, Delsol C, Dragani R, Fuentes M, Geer A J, Haimberger L, Healy S B, Hersbach H, Hólm E V, Isaksen L, Kållberg P, Köhler M, Matricardi M, McNally A P, Monge-Sanz B M, Morcrette J J, Park B K, Peubey C, de Rosnay P, Tavolato C, Thépaut J N and Vitart F 2011 The ERA-Interim reanalysis: configuration and performance of the data assimilation system *Quarterly Journal of the Royal Meteorological Society* **137** 553-97

Etheridge D M, Steele L P, Francey R J and Langenfelds R L 1998 Atmospheric methane between 1000 A.D. and present: Evidence of anthropogenic emissions and climatic variability *Journal of Geophysical Research: Atmospheres* **103** 15979-93

Gelaro R, McCarty W, Suárez M J, Todling R, Molod A, Takacs L, Randles C A, Darmenov A, Bosilovich M G, Reichle R, Wargan K, Coy L, Cullather R, Draper C, Akella S, Buchard V, Conaty A, Silva A M d, Gu W, Kim G-K, Koster R, Lucchesi R, Merkova D, Nielsen J E, Partyka G, Pawson S, Putman W, Rienecker M, Schubert S D, Sienkiewicz M and Zhao B 2017 The Modern-Era Retrospective Analysis for Research and Applications, Version 2 (MERRA-2) *Journal of Climate* **30** 5419-54

Geng S, Penning de Vries F W T and Supit I 1986 A simple method for generating daily rainfall data *Agricultural and Forest Meteorology* **36** 363-76

Harris I, Jones P D, Osborn T J and Lister D H 2014 Updated high-resolution grids of monthly climatic observations – the CRU TS3.10 Dataset *International Journal of Climatology* **34** 623-42

Helmig D, Rossabi S, Hueber J, Tans P, Montzka S A, Masarie K, Thoning K, Plass-Duelmer C, Claude A, Carpenter L J, Lewis A C, Punjabi S, Reimann S, Vollmer M K, Steinbrecher R, Hannigan J W, Emmons L K, Mahieu E, Franco B, Smale D, and Pozzer A 2016 Reversal of global atmospheric ethane and propane trends largely due to US oil and natural gas production. Nature Geoscience 9:490.

Hodson E L, Poulter B, Zimmermann N E, Prigent C and Kaplan J O 2011 The El Niño–Southern Oscillation and wetland methane interannual variability *Geophysical Research Letters* **38** L08810

Hopcroft P O, Valdes P J, O'Connor F M, Kaplan J O and Beerling D J 2017 Understanding the glacial methane cycle *Nature Communications* **8** 14383

Hurtt C G, Chini L P, Frolking S, Betts R A, Feddem J, Fischer G, Fisk J P, Hibbard K, Houghton R A, Janetos A, Jones C D, Kindermann G, Kinoshita T, Klein Goldewijk K, Riahi K, Shevliakova E, Smith S, Stehfest E, Thomson A, Thornton P, van Vuuren D P, Wang Y P 2011 Harmonization of land-use scenarios for the period 1500–2100: 600 years of global gridded annual land-use transitions, wood harvest, and resulting secondary lands. Climatic Change 109, 117.

IPCC 2013 *Climate Change 2013: The Physical Science Basis. Contribution of Working Group I to the Fifth Assessment Report of the Intergovernmental Panel on Climate Change* (Cambridge, United Kingdom and New York, NY, USA: Cambridge University Press)

Jiménez-Muñoz J C, Mattar C, Barichivich J, Santamaría-Artigas A, Takahashi K, Malhi Y, Sobrino J A and Schrier G V D 2016 Record-breaking warming and extreme drought in the Amazon rainforest during the course of El Niño 2015–2016 *Scientific Reports* **6** 33130

Kirschke S, Bousquet P, Ciais P, Saunois M, Canadell J G, Dlugokencky E J, Bergamaschi P, Bergmann D, Blake D R, Bruhwiler L, Cameron-Smith P, Castaldi S, Chevallier F, Feng L, Fraser A, Heimann M, Hodson E L, Houweling S, Josse B, Fraser P J, Krummel P B, Lamarque J-F, Langenfelds R L, Le Quere

C, Naik V, O'Doherty S, Palmer P I, Pison I, Plummer D, Poulter B, Prinn R G, Rigby M, Ringeval B, Santini M, Schmidt M, Shindell D T, Simpson I J, Spahni R, Steele L P, Strode S A, Sudo K, Szopa S, van der Werf G R, Voulgarakis A, van Weele M, Weiss R F, Williams J E and Zeng G 2013 Three decades of global methane sources and sinks *Nature Geosci* **6** 813-23

Kobayashi S, Ota Y, Harada Y, Ebita A, Moriya M, Onoda H, Onogi K, Kamahori H, Kobayashi C, Endo H, Miyaoka K and Takahashi K 2015 The JRA-55 Reanalysis: General Specifications and Basic Characteristics *Journal of the Meteorological Society of Japan. Ser. II* **93** 5-48

L'Heureux M L, Takahashi K, Watkins A B, Barnston A G, Becker E J, Di Liberto T E, Gamble F, Gottschalck J, Halpert M S, Huang B, Mosquera-Vásquez K and Wittenberg A T 2016 Observing and Predicting the 2015/16 El Niño *Bulletin of the American Meteorological Society* **98** 1363-82

Landerer F W and Swenson S C 2012 Accuracy of scaled GRACE terrestrial water storage estimates *Water Resources Research* **48** W04531

Lehner B and Döll P 2004 Development and validation of a global database of lakes, reservoirs and wetlands *Journal of Hydrology* **296** 1-22

Lim Y-K, Kovach R M, Pawson S and Vernieres G 2017 The 2015/16 El Niño Event in Context of the MERRA-2 Reanalysis: A Comparison of the Tropical Pacific with 1982/83 and 1997/98 *Journal of Climate* **30** 4819-42

Liu J, Bowman K W, Schimel D S, Parazoo N C, Jiang Z, Lee M, Bloom A A, Wunch D, Frankenberg C, Sun Y, O'Dell C W, Gurney K R, Menemenlis D, Gierach M, Crisp D and Eldering A 2017 Contrasting carbon cycle responses of the tropical continents to the 2015–2016 El Niño *Science* **358**

MacFarling Meure C, Etheridge D, Trudinger C, Steele P, Langenfelds R, van Ommen T, Smith A and Elkins J 2006 Law Dome CO_2, CH_4 and N_2O ice core records extended to 2000 years BP *Geophysical Research Letters* **33** L14810

McNorton J, Gloor E, Wilson C, Hayman G D, Gedney N, Comyn-Platt E, Marthews T, Parker R J, Boesch H and Chipperfield M P 2016 Role of regional wetland emissions in atmospheric methane variability *Geophysical Research Letters* 43 11,433–11,444

Melton J R, Wania R, Hodson E L, Poulter B, Ringeval B, Spahni R, Bohn T, Avis C A, Beerling D J, Chen G, Eliseev A V, Denisov S N, Hopcroft P O, Lettenmaier D P, Riley W J, Singarayer J S, Subin Z M, Tian H, Zürcher S, Brovkin V, van Bodegom P M, Kleinen T, Yu Z C and Kaplan J O 2013 Present state of global wetland extent and wetland methane modelling: conclusions from a model inter-comparison project (WETCHIMP) *Biogeosciences* **10** 753-88

Montzka S A, Krol M, Dlugokencky E, Hall B, Jöckel P and Lelieveld J 2011 Small Interannual Variability of Global Atmospheric Hydroxyl *Science* **331** 67-9

Nachtergaele F, Van Velthuizen H, Verelst L, Batjes N, Dijkshoorn K, Van Engelen V, Fischer G, Jones A, Montanarella L, and Petri M 2008: Harmonized world soil database, FAO, Rome, Italy and IIASA, Laxenburg, Austria.

Nisbet E G, Dlugokencky E J and Bousquet P 2014 Methane on the Rise—Again *Science* **343** 493-5

Nisbet E G, Dlugokencky E J, Manning M R, Lowry D, Fisher R E, France J L, Michel S E, Miller J B, White J W C, Vaughn B, Bousquet P, Pyle J A, Warwick N J, Cain M, Brownlow R, Zazzeri G, Lanoisellé M, Manning A C, Gloor E, Worthy D E J, Brunke E G, Labuschagne C, Wolff E W and Ganesan A L 2016 Rising atmospheric methane: 2007–2014 growth and isotopic shift *Global Biogeochemical Cycles* **30** 1356-70

Pandey S, Houweling S, Krol M, Aben I, Monteil G, Nechita-Banda N, Dlugokencky E J, Detmers R, Hasekamp O, Xu X, Riley W J, Poulter B, Zhang Z, McDonald K C, White J W C, Bousquet P and Röckmann T 2017 Enhanced methane emissions from tropical wetlands during the 2011 La Niña *Scientific Reports* **7** 45759

Philander SGH 1990 El Nino, La Nina, and the Southern Oscillation (Academic London)

Pison I, Ringeval B, Bousquet P, Prigent C and Papa F 2013 Stable atmospheric methane in the 2000s: key-role of emissions from natural wetlands *Atmos. Chem. Phys.* **13** 11609-23

Poulter B, Bousquet P, Canadell G J, Ciais P, Peregon A, Saunois M, Arora K V, Beerling J D, Brovkin V, Jones D C, Joos F, Gedney N, Ito A, Kleinen T, Koven D C, McDonald K, Melton R J, Peng C, Peng S, Prigent C, Schroeder R, Riley J W, Saito M, Spahni R, Tian H, Taylor L, Viovy N, Wilton D, Wiltshire A, Xu X, Zhang B, Zhang Z and Zhu Q 2017 Global wetland contribution to 2000–2012 atmospheric methane growth rate dynamics *Environmental Research Letters* **12** 094013

Poulter B, Frank D C, Hodson E L and Zimmermann N E 2011 Impacts of land cover and climate data selection on understanding terrestrial carbon dynamics and the CO_2 airborne fraction *Biogeosciences* **8** 2027-36

Prentice I C, Martin T S and Wolfgang C 1993 A simulation model for the transient effects of climate change on forest landscapes *Ecological Modelling* **65** 51-70

Prigent C, Papa F, Aires F, Jimenez C, Rossow W B and Matthews E 2012 Changes in land surface water dynamics since the 1990s and relation to population pressure *Geophysical Research Letters* **39** L08403

Quiquet A, Archibald A T, Friend A D, Chappellaz J, Levine J G, Stone E J, Telford P J and Pyle J A 2015 The relative importance of methane sources and sinks over the Last Interglacial period and into the last glaciation *Quaternary Science Reviews* **112** 1-16

Rigby M, Montzka S A, Prinn R G, White J W C, Young D, O'Doherty S, Lunt M F, Ganesan A L, Manning A J, Simmonds P G, Salameh P K, Harth C M, Mühle J, Weiss R F, Fraser P J, Steele L P, Krummel P B, McCulloch A and Park S 2017 Role of atmospheric oxidation in recent methane growth *Proceedings of the National Academy of Sciences* **114** 5373-7

Ringeval B, Houweling S, van Bodegom P M, Spahni R, van Beek R, Joos F and Röckmann T 2014 Methane emissions from floodplains in the Amazon Basin: challenges in developing a process-based model for global applications *Biogeosciences* **11** 1519-58

Rodell M, Famiglietti J S, Wiese D N, Reager J T, Beaudoing H K, Landerer F W, Lo M H, 2018 Emerging trends in global freshwater availability. Nature.

Sakumura C, Bettadpur S and Bruinsma S 2014 Ensemble prediction and intercomparison analysis of GRACE time-variable gravity field models *Geophysical Research Letters* **41** 1389-97

Saunois M, Jackson R B, Bousquet P, Poulter B and Canadell J G 2016 The growing role of methane in anthropogenic climate change *Environmental Research Letters* **11** 120207

Schaefer H, Fletcher S E M, Veidt C, Lassey K R, Brailsford G W, Bromley T M, Dlugokencky E J, Michel S E, Miller J B, Levin I, Lowe D C, Martin R J, Vaughn B H and White J W C 2016 A 21st century shift from fossil-fuel to biogenic methane emissions indicated by $^{13}CH_4$ *Science* **352** 80-4

Schroeder R, McDonald K, Chapman B, Jensen K, Podest E, Tessler Z, Bohn T and Zimmermann R 2015 Development and Evaluation of a Multi-Year Fractional Surface Water Data Set Derived from Active/Passive Microwave Remote Sensing Data *Remote Sensing* **7** 15843

Schwietzke S, Sherwood O A, Bruhwiler L M P, Miller J B, Etiope G, Dlugokencky E J, Michel S E, Arling V A, Vaughn B H, White J W C and Tans P P 2016 Upward revision of global fossil fuel methane emissions based on isotope database *Nature* **538** 88-91

Sitch S, Smith B, Prentice I C, Arneth A, Bondeau A, Cramer W, Kaplan J O, Levis S, Lucht W, Sykes M T, Thonicke K and Venevsky S 2003 Evaluation of ecosystem dynamics, plant geography and terrestrial carbon cycling in the LPJ dynamic global vegetation model *Global Change Biology* **9** 161-85

Sun, Q, Miao C, Duan Q, Ashouri H, Sorooshian S, and Hsu K L 2018 A Review of Global Precipitation Data Sets: Data Sources, Estimation, and Intercomparisons. Reviews of Geophysics 56:79-107.

Thoning K W, Tans P P and Komhyr W D 1989 Atmospheric carbon dioxide at Mauna Loa Observatory: 2. Analysis of the NOAA GMCC data, 1974–1985 *Journal of Geophysical Research: Atmospheres* **94** 8549-65

Thornton B F, Wik M and Crill P M 2016 Double counting challenges the accuracy of high latitude methane inventories *Geophysical Research Letters* 43 12569-12577

Tian H, Lu C, Ciais P, Michalak A M, Canadell J G, Saikawa E, Huntzinger D N, Gurney K R, Sitch S, Zhang B, Yang J, Bousquet P, Bruhwiler L, Chen G, Dlugokencky E, Friedlingstein P, Melillo J, Pan S, Poulter B, Prinn R, Saunois M, Schwalm C R and Wofsy S C 2016 The terrestrial biosphere as a net source of greenhouse gases to the atmosphere *Nature* **531** 225-8

Turner A J, Frankenberg C, Wennberg P O and Jacob D J 2017 Ambiguity in the causes for decadal trends in atmospheric methane and hydroxyl *Proceedings of the National Academy of Sciences* **114** 5367-72

Whitburn S, Van Damme M, Clarisse L, Turquety S, Clerbaux C and Coheur P F 2016 Doubling of annual ammonia emissions from the peat fires in Indonesia during the 2015 El Niño *Geophysical Research Letters* **43** 11,007-11,14

Wolf J, Asrar G R and West T O 2017 Revised methane emissions factors and spatially distributed annual carbon fluxes for global livestock *Carbon Balance and Management* **12** 16

Wolter K and Timlin M S 1998 Measuring the strength of ENSO events: How does 1997/98 rank? *Weather* **53** 315-24

Worden J, Wecht K, Frankenberg C, Alvarado M, Bowman K, Kort E, Kulawik S, Lee M, Payne V and Worden H 2013 CH_4 and CO distributions over tropical fires during October 2006 as observed by the Aura TES satellite instrument and modeled by GEOS-Chem *Atmos. Chem. Phys.* **13** 3679-92

Xiong X, Han Y, Liu Q and Weng F 2016 Comparison of Atmospheric Methane Retrievals From AIRS and IASI *IEEE Journal of Selected Topics in Applied Earth Observations and Remote Sensing* **9** 3297-303

Fang Y, Michalak M A, Schwalm R C, Huntzinger N D, Berry A J, Ciais P, Piao S, Poulter B, Joshua F B, Cook B R, Hayes D, Huang M, Ito A, Jain A, Lei H, Lu C, Mao J, Parazoo C N, Peng S, Ricciuto M D, Shi X, Tao B, Tian H, Wang W, Wei Y, Yang J 2017 Global land carbon sink response to temperature and precipitation varies with ENSO phase. *Environmental Research Letters* 12, 064007.

Zhang G, Xiao X, Biradar C M, Dong J, Qin Y, Menarguez M A, Zhou Y, Zhang Y, Jin C, Wang J, Doughty R B, Ding M and Moore Iii B 2017a Spatiotemporal patterns of paddy rice croplands in China and India from 2000 to 2015 *Science of The Total Environment* **579** 82-92

Zhang Z, Zimmermann N E, Kaplan J O and Poulter B 2016 Modeling spatiotemporal dynamics of global wetlands: comprehensive evaluation of a new sub-grid TOPMODEL parameterization and uncertainties *Biogeosciences* **13** 1387-408

Zhang Z, Zimmermann N E, Stenke A, Li X, Hodson E L, Zhu G, Huang C and Poulter B 2017b Emerging role of wetland methane emissions in driving 21st century climate change *Proceedings of the National Academy of Sciences* **114** 9647-52

Zhu Q, Peng C, Ciais P, Jiang H, Liu J, Bousquet P, Li S, Chang J, Fang X, Zhou X, Chen H, Liu S, Lin G, Gong P, Wang M, Wang H, Xiang W and Chen J 2017 Interannual variation in methane emissions from tropical wetlands triggered by repeated El Niño Southern Oscillation *Global Change Biology* 23 4706-4716

Zona D, Gioli B, Commane R, Lindaas J, Wofsy S C, Miller C E, Dinardo S J, Dengel S, Sweeney C, Karion A, Chang R Y-W, Henderson J M, Murphy P C, Goodrich J P, Moreaux V, Liljedahl A, Watts J D, Kimball J S, Lipson D A and Oechel W C 2016 Cold season emissions dominate the Arctic tundra methane budget *Proceedings of the National Academy of Sciences* **113** 40-5

Figures:

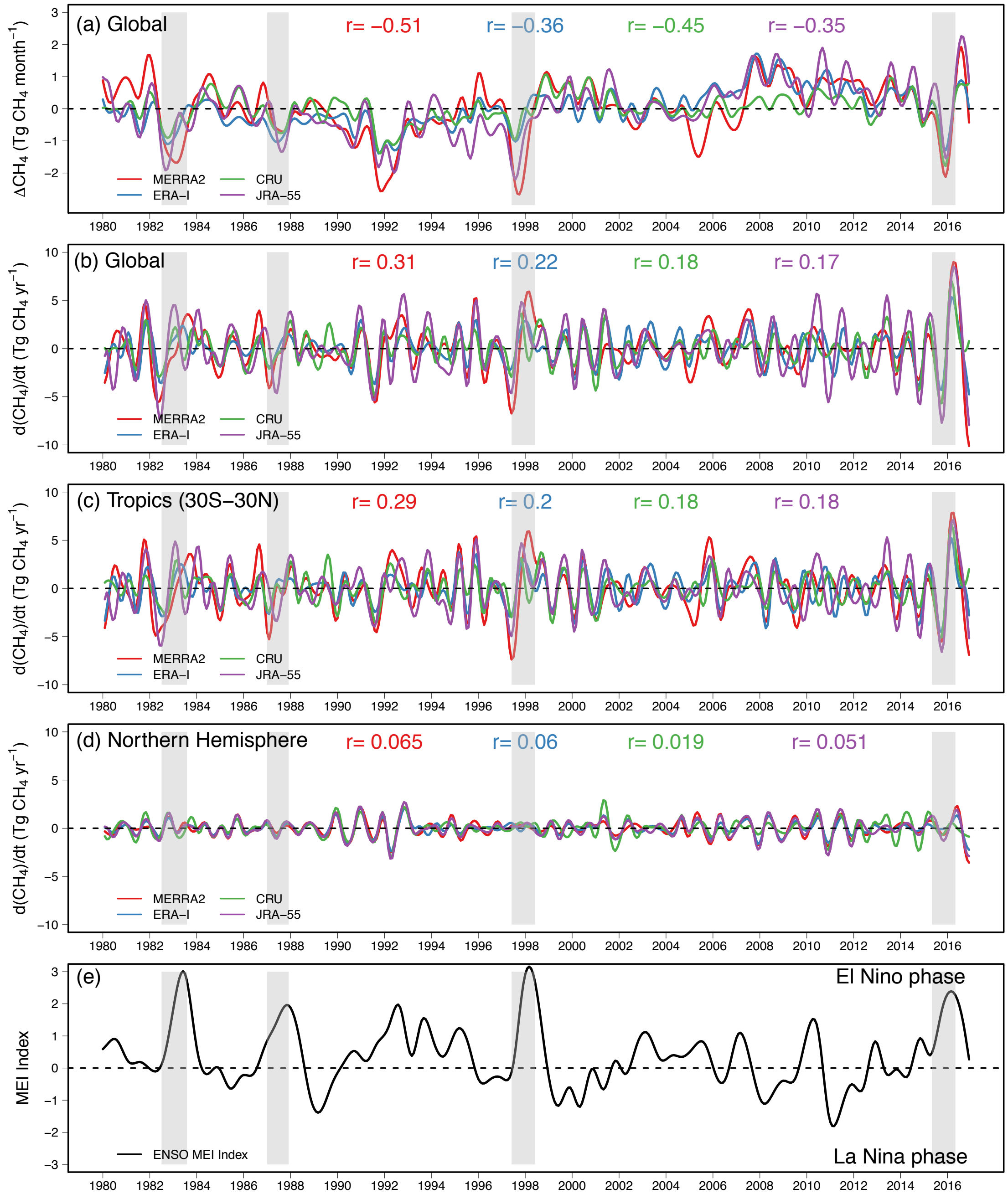

Figure 1. Global anomalies of monthly wetland CH_4 emissions (a) and instantaneous growth rates of wetland CH_4 emission anomalies from 1980 to 2016 for the Global (b), Tropics (middle, 30°S-30°N) (c), and Northern Hemisphere (bottom, >30°N) (d). The global anomalies of wetland CH_4 emissions were calculated relative to monthly average from 1980-2016. The instantaneous growth rate for each simulation is a time derivative of the smoothed monthly CH_4 anomalies using spline functions. The Spearman rank correlation coefficients between the multivariate ENSO index (MEI) and monthly wetland anomalies were derived from cross correlation analyses

(Figure S1) at 3 month lags (Lag= -3), with different colors corresponding to specific runs. Shaded grey areas represent the strong El Niño phases with MEI strength > 60 according to MEI ranks (https://www.esrl.noaa.gov/psd/enso/mei/rank.html, last access at January 2018).

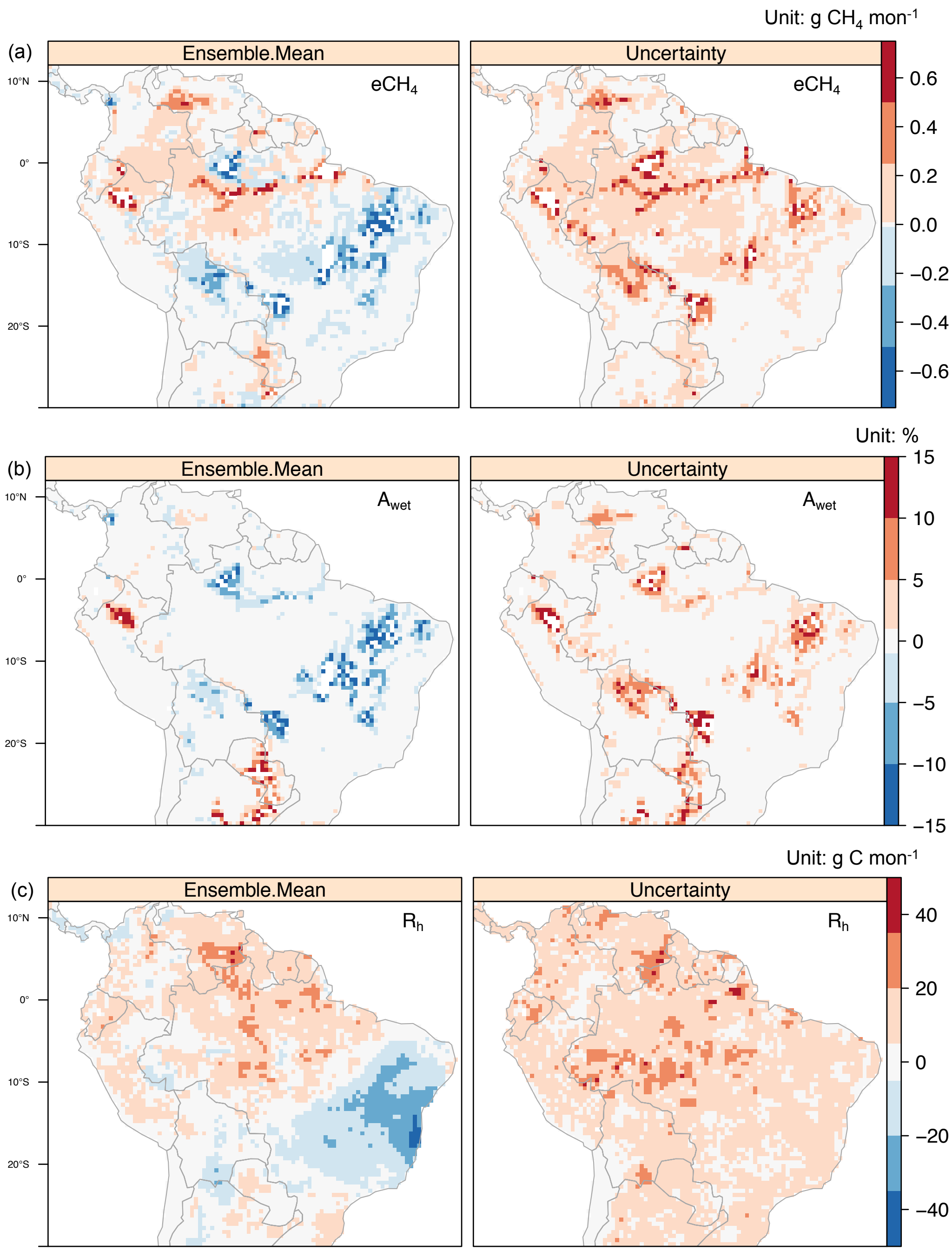

Figure 2. Spatial distributions of seasonal ensemble mean anomalies in wetland CH_4 emissions (a: eCH_4, Unit: g CH_4 m^{-2} mon^{-1}), inundated areas (b: A_{wet}, Unit: %), and heterotrophic respiration (c: R_h, Unit: g C m^{-2} mon^{-1}) of the greater Amazonia region for the March-April-May season, 2016, where eCH_4 shows the highest growth rate during the 2015-2016 ENSO event. The anomalies are calculated as seasonal means during the MAM season of 2016 relative to average over the period of 1980-2016 level, with the uncertainty calculated as one-standard deviation from the four simulations forced by each meteorological dataset.

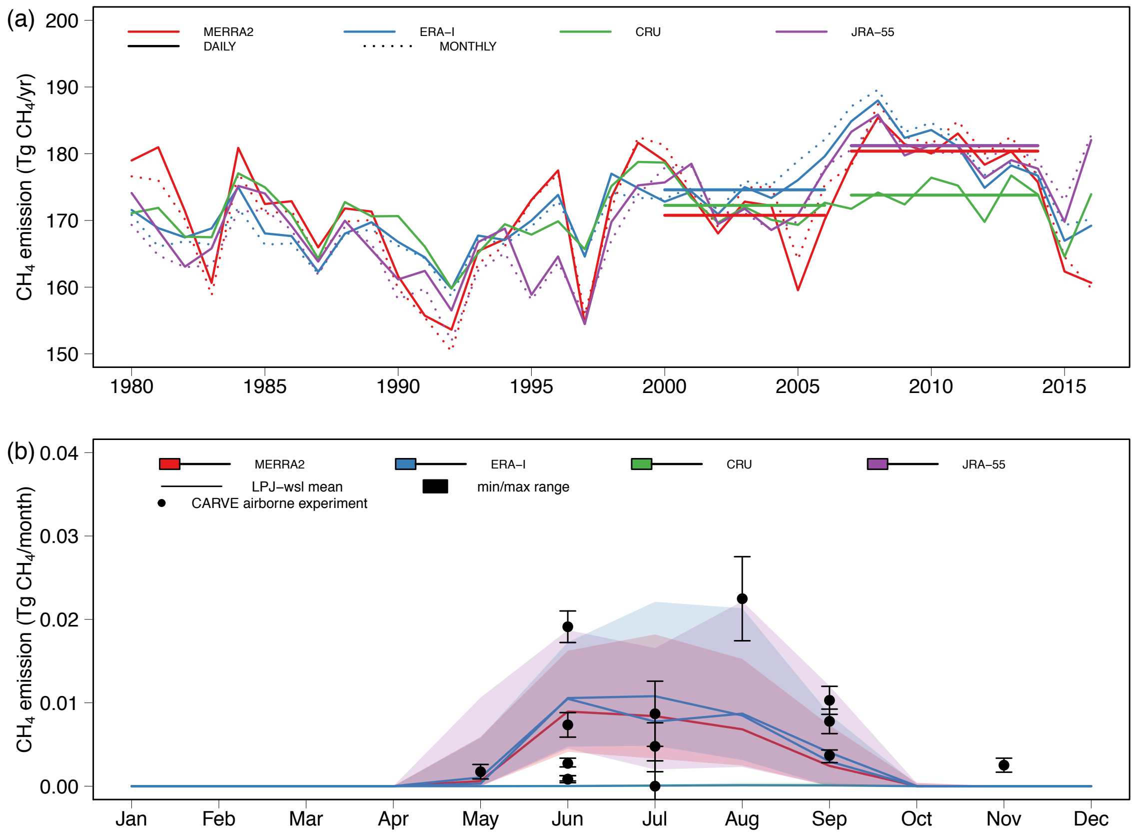

Figure 3. Simulated temporal patterns of CH_4 from all model experiments (see details in Table 1). (a) Time series of annual CH_4 emissions using climate forcings with daily and monthly temporal resolution. The daily forcings were aggregated to monthly values to evaluate the influence of daily variations of climate variables on CH_4 estimations. Solid and dotted lines represent daily and monthly inputs, respectively. The horizontal lines represent averaged annual CH_4 emissions for two time periods, 2000-2006 and 2007-2014, with the different colors representing different climate forcings. (b) Comparison between the seasonal cycle of LPJ-wsl simulated monthly CH_4 fluxes (solid line) using different climate forcings, with min/maximum range (areal shaded) over the Northern Slope of Alaska for 2012-2014 in comparison to the observed regional CH_4 fluxes (dots) estimated from analysis of 15 aircraft flights by the National Aeronautics and Space Administration's Carbon in Arctic Vulnerability Experiment (CARVE).

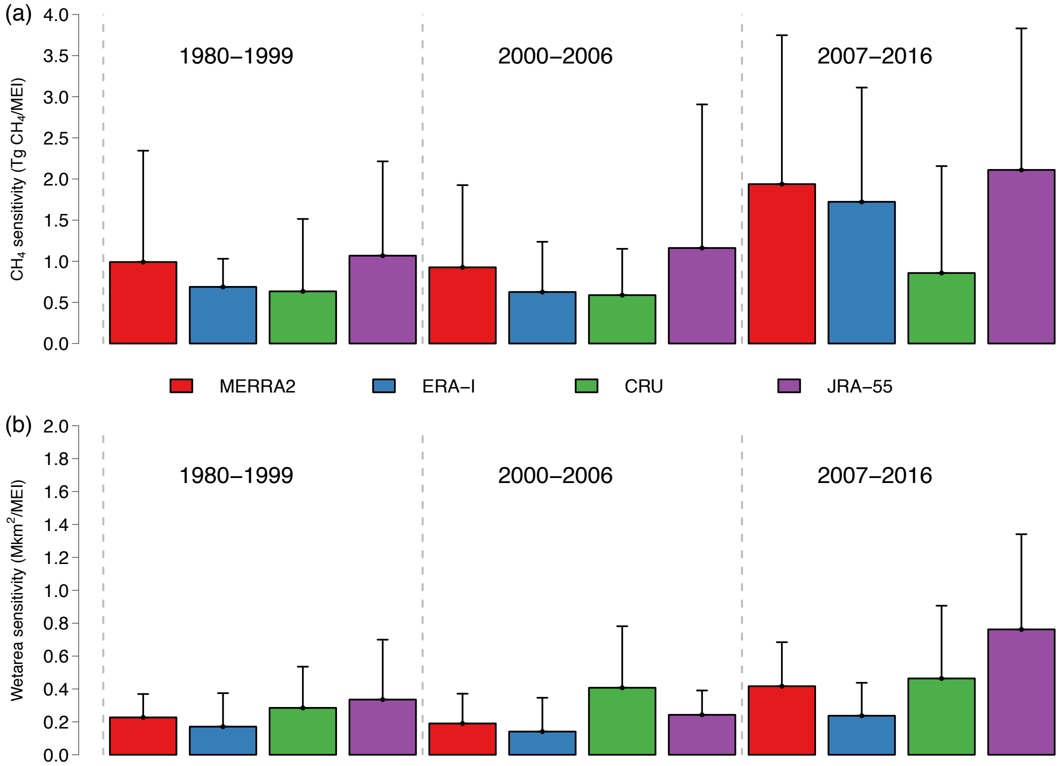

Figure 4. Sensitivity of (a) wetland CH_4 anomalies (Unit: Tg CH_4 /yr/MEI) and (b) wetland area anomalies for the tropics (Unit: Mkm^2/yr/MEI; Mkm^2 = 10^6 km^2) to global ENSO strength for the period of 1980-1999, 2000-2006, and 2007-2016. The sensitivity metric is calculated as the ratio of averaged annual cumulative anomalies of wetland CH_4 emissions and wetland areas to the MEI index. Bars represent the modeled sensitivity from experiments with different forcing datasets, and the error bars represent one standard deviation.

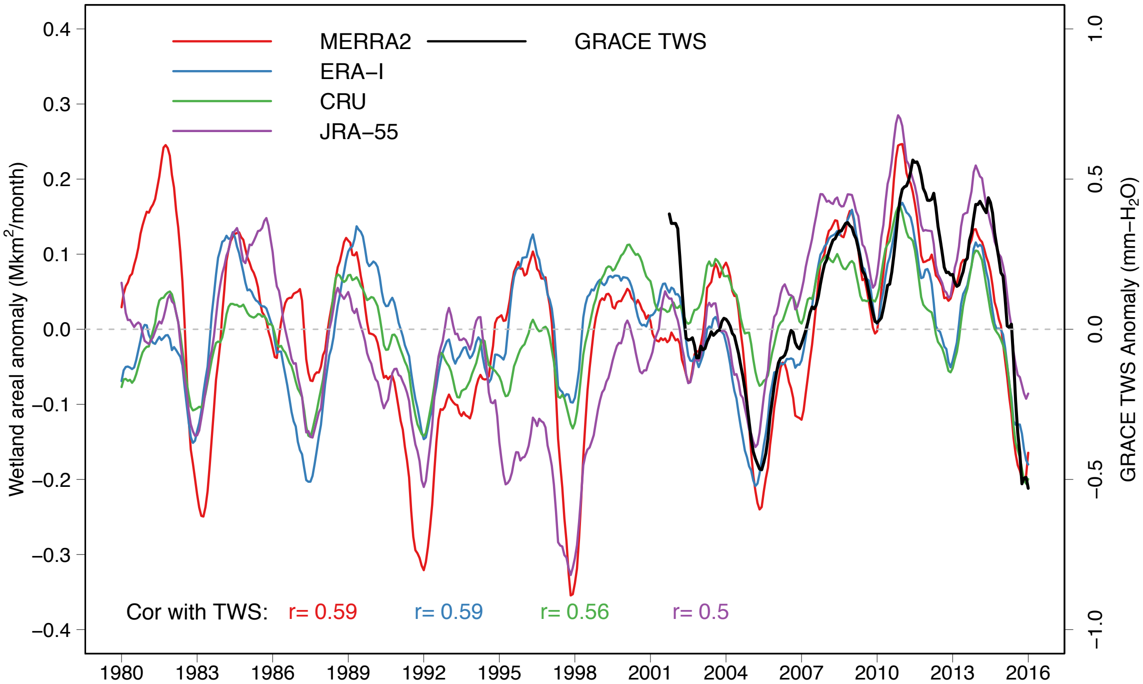

Figure 5. Trends of simulated wetland areal anomalies (Unit: Mkm^2/month; Mkm^2=10^6 km^2) for the tropics (30°S-30°N) compared to area-weighted average terrestrial water storage (TWS; Unit: mm-H_2O) from the ensemble mean of GRACE satellite measurement. The wetland anomalies were calculated relative to the monthly mean of 1980-2016, while TWS anomalies were relative to means of the 2004-2009 period. The fitted trends were calculated by smoothing the monthly anomalies with a 12-month moving average. The Spearman rank correlation coefficients between model and TWS are given for each simulation with different climate forcings in corresponding colors.

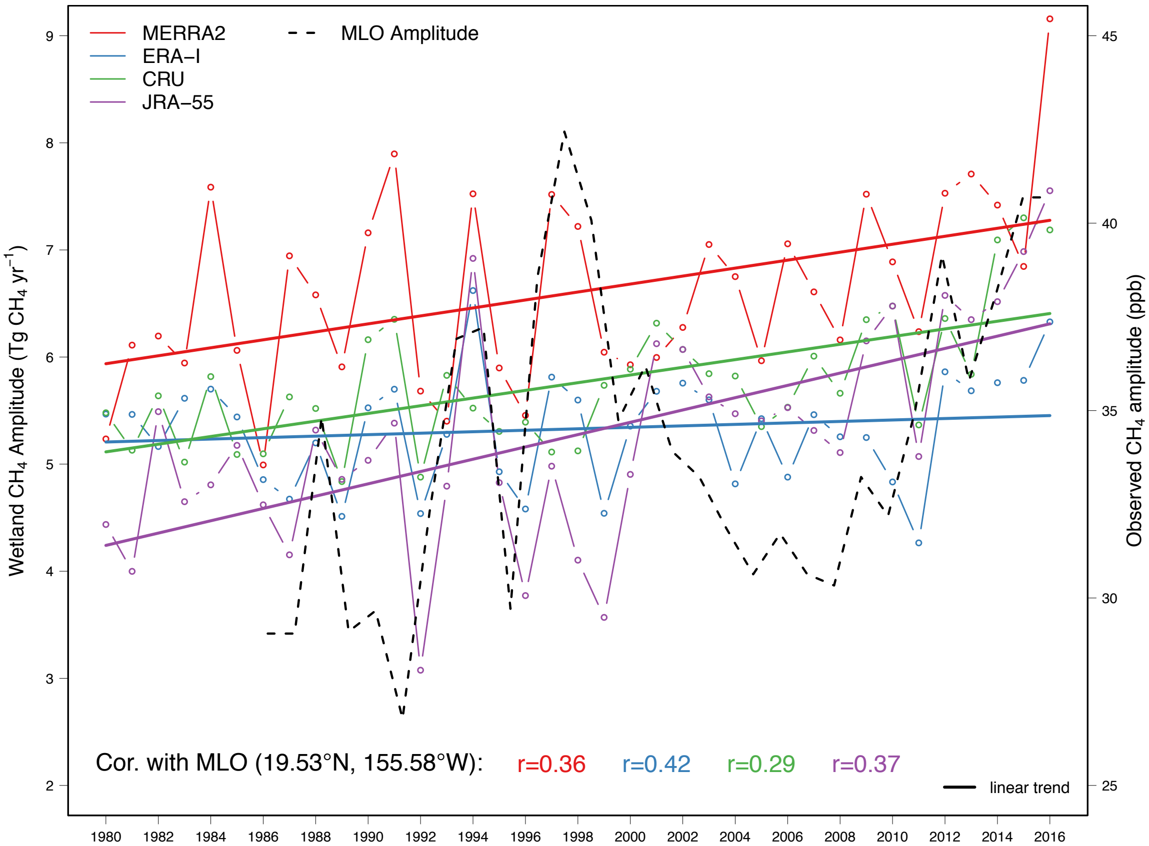

Figure 6. Time series of the seasonal amplitudes of global CH_4 fluxes. The seasonal amplitude of CH_4 fluxes (dashed dotted line) is calculated as the difference between maxima and minima of simulated monthly CH_4 emissions. The dashed black line represents observed peak-to-through seasonal amplitude of atmospheric CH_4 concentration at Mauna Loa observational station. The solid lines represent linear fitted long-term trends of the seasonal CH_4 cycle with Spearman rank correlation coefficients between models and observed amplitudes listed for each model runs in corresponding colors.

Tables:

Table 1. Model experiment descriptions. Climatic variables T, P, SW, LW, CLD, and WETD represent temperature, precipitation, shortwave radiation, longwave radiation, cloud cover, and wet days respectively.

Run ID number	Forcing	Temporal Resolution	Climatic Variables	Time periods
i	MERRA2	Daily	T, P, SW, LW	1980-2016
ii	MERRA2	Monthly	T, P, SW, LW*	1980-2016
iii	ERA-I	Daily	T, P, SW, LW	1980-2016
iv	ERA-I	Monthly	T, P, SW, LW	1980-2016
v	JRA-55	Daily	T, P, SW, LW	1980-2016
vi	JRA-55	Monthly	T, P, SW, LW*	1980-2016
vii	CRU	Monthly	T, P, CLD, WETD	1901-2016

*CLD and WETD are from CRU for comparison

Table 2. Summary of mean annual CH_4 emissions of the Tropics (30°S-30°N, denoted as TRO), the Northern Extratropics (denoted as NET), and the Southern Extratropics (denoted SET) for 2000-2006, and 2007-2014 from simulations with daily meteorological forcings MERRA2, ERA-I, and JRA-55 and with a spatial-interpolated climate dataset CRU that is based on interpolations from meteorological stations.

Time period	Forcing	eCH_4 (Tg CH_4 yr^{-1})			
		TRO	NET	SET	Global
2000-2006	CRU	138.1	32.3	1.8	172.2
	MERRA2	136.1	32.5	2.1	170.7
	ERA-I	142.3	26.6	1.9	170.9
	JRA-55	141.5	29.8	1.8	173.1
2007-2014	CRU	139.1	33.0	1.7	173.8
	MERRA2	145.6	32.8	1.9	180.3
	ERA-I	148.6	27.0	1.8	177.4
	JRA-55	147.7	31.1	1.8	180.6

Supplementary Information:

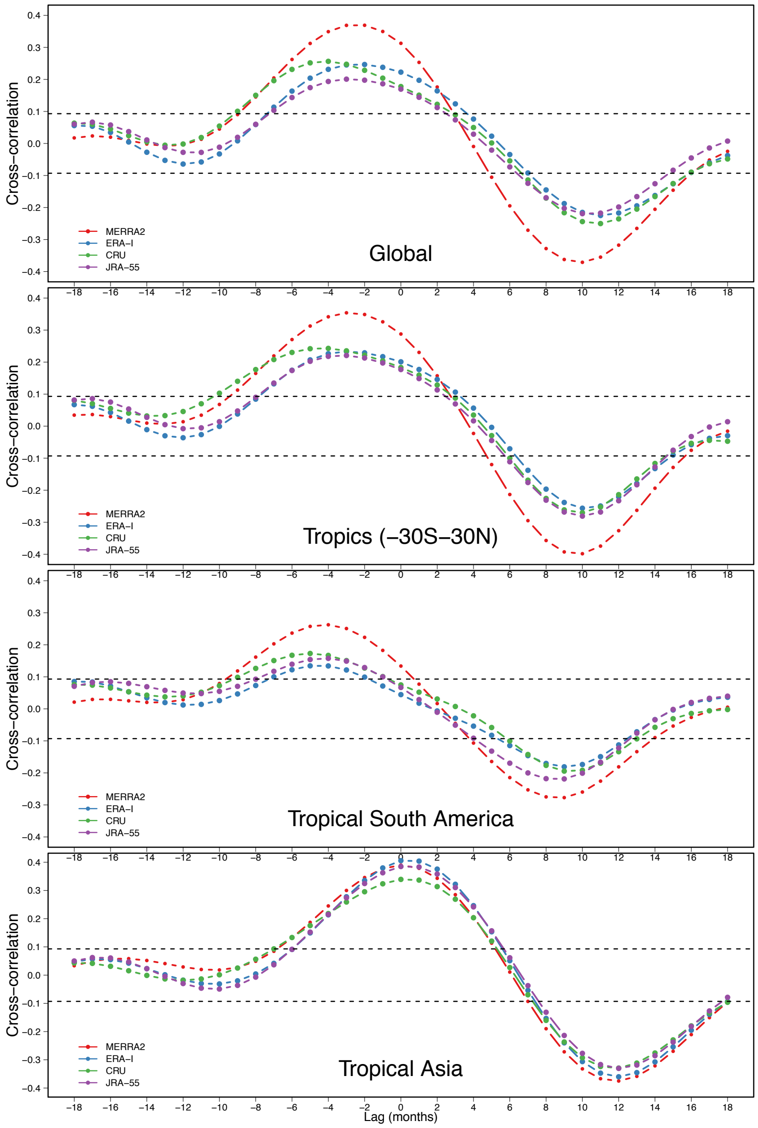

Figure S1. Cross-correlation analysis between ENSO MEI index and instantaneous growth rate of wetland CH_4 anomalies (calculated as time derivative of deseasonalized monthly wetland CH_4 emissions) from four simulations with different forcings (MERRA2, ERA-I, CRU, JRA-55). Dashed horizontal blue lines in all panels represent the 95% confidence interval.

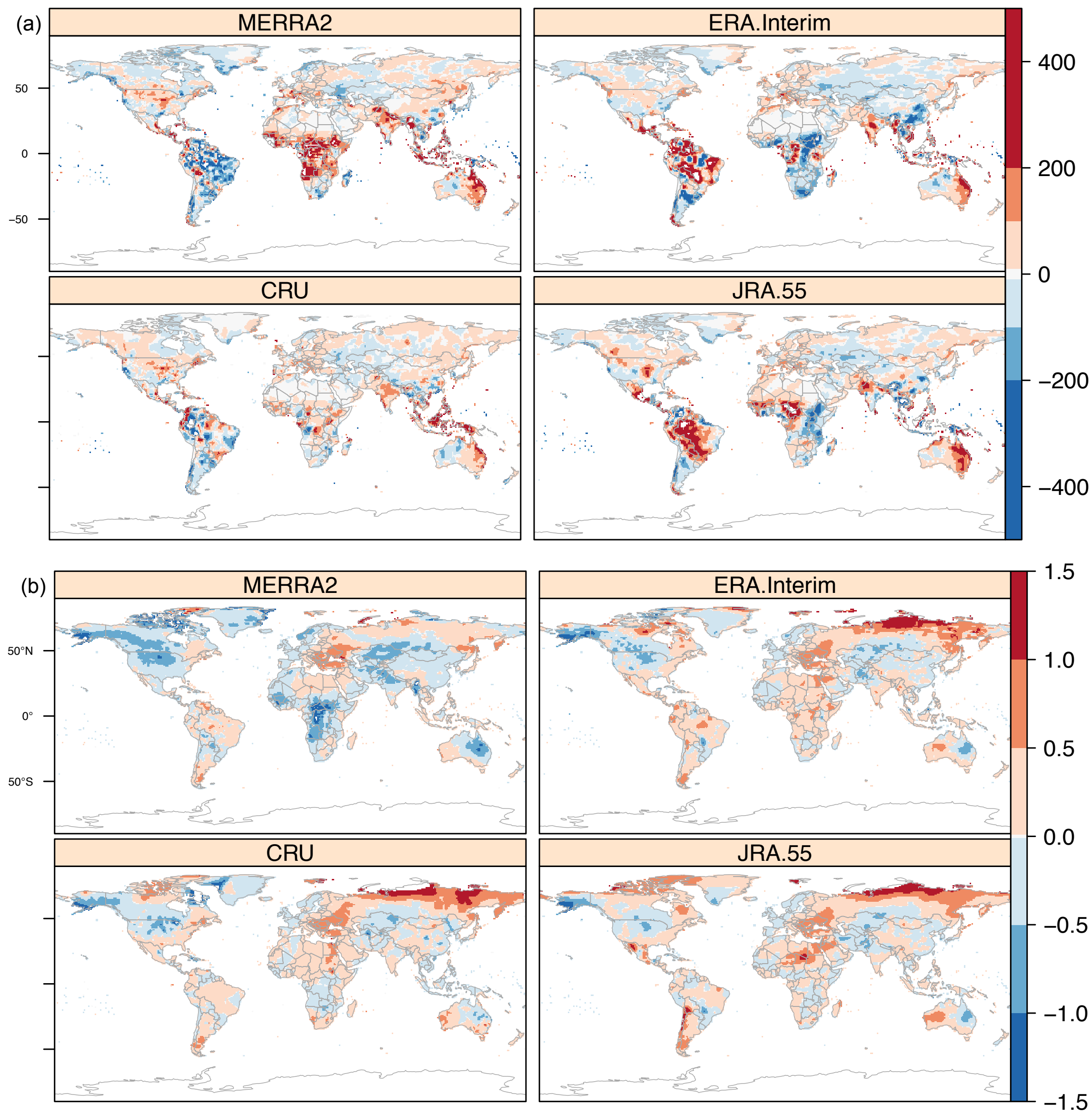

Figure S2. Spatial distribution of the mean difference in (a) precipitation (Unit: mm yr^{-1}) and (b) temperature (Unit: °C yr^{-1}) between 2007-2014 and 2000-2006 for MERRA2 and ERA-I.

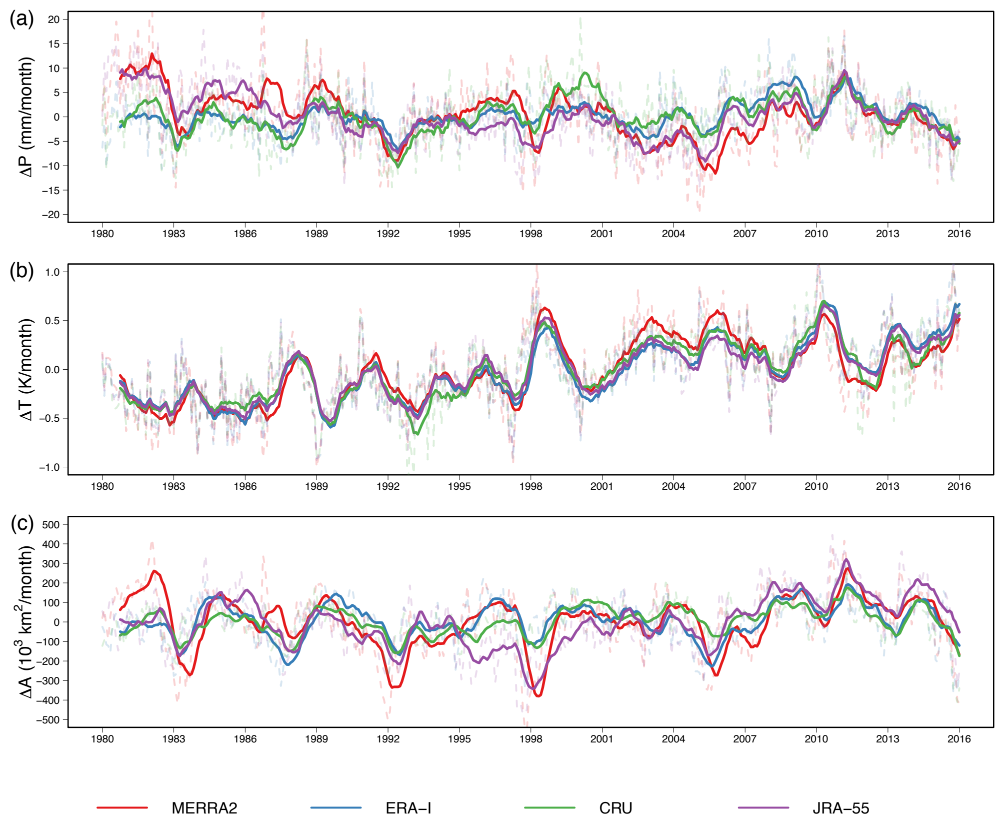

Figure S3. Time series of climate variables and simulated wetland area for the monthly anomalies of (a) precipitation (ΔP), (b) temperature (ΔT), and (c) wetland area (ΔA) in the tropics (30°S-30°N). Monthly anomalies were estimated relative to corresponding long-term monthly mean (1980-2016). Dashed and solid lines represent the monthly anomaly and 12-month moving average respectively.